

# Dynamics and Morphology of the Milky Way Spiral Arms from the Metallicity Distribution and Radial Mixing

L.A. Martinez-Medina <sup>\*</sup>, B. Pichardo, A. Peimbert, & L. Carigi

*Instituto de Astronomía, Universidad Nacional Autónoma de México, A.P. 70–264, 04510, México, CDMX, México*

1 September 2021

## ABSTRACT

Albeit radial migration must be a ubiquitous process in disc galaxies, its significance in the evolution of stellar discs is not always reflected through global trends. However, there are other key observables, such as the metallicity distribution function (MDF), that may shed some light in this matter. We argue that the shape of the MDF not only tells us whether the stellar disc experienced radial migration, but it also contains important clues on the structure that triggered it. Specifically, the MDF contains information about the dynamics and morphology of the spiral pattern. To constrain the spiral parameters, we have included a detailed chemical tagging in our simulations; this allows us to produce a restriction of the structural parameters of the spiral arms in the Milky Way as well as a method to constrain chemical evolution models towards the center of the Galactic disc, where no chemical model provides information. We also found that it is unlikely that the Sun was formed near its current galactocentric position, therefore it might be inaccurate to consider the Sun as representative of the chemical abundances in the solar neighborhood. We also show that a stellar disc of the Milky Way, after evolving dynamically and chemically for 5 Gyr, preserves 80% of its original global metallicity gradient despite having suffered important heating and radial migration; this means that the presence of a metallicity gradient in a given galaxy, does not guarantee that radial mixing has not played a role in its evolution.

**Key words:** Galaxy: disc — Galaxy: evolution — Galaxy: kinematics and dynamics — Galaxy: structure — Galaxy: abundances — Sun: abundances

## 1 INTRODUCTION

It has been a long journey since the first clues of the discrepancy between our ideal picture, of a well behaved axisymmetric Galactic disc, and observations were revealed. In this ideal scenario stellar orbits were approximately circular, the large scale non-axisymmetric structures (spiral arms and bar) had negligible effects on the dynamics, and a perfect correlation between age and metallicity of a star could be found for a given Galactic region. Some of the pioneering work noticing the discrepancy between the required characteristics for that ideal scenario and reality, comes with Grenon (1972, 1989). He found in the solar neighbourhood a super metal-rich stellar population that exhibits the abundance of chemical elements and kinematics of the central regions of the Galaxy; since that time a possible stellar mixing that somehow was taking place in the Galaxy was proposed (e.g. Wielen 1977). Likewise, Edvardsson et al. (1993) found a poor correlation between age and metallicity for stars in the Solar neighbourhood from the thin disc. Later

on Francois & Matteucci (1993) produced the first analysis of the relevance of radial mixing on the chemical properties of the Galaxy; by using the spread observed in the age metallicity relation and in the  $[\alpha/\text{Fe}]$  vs.  $[\text{Fe}/\text{H}]$  relation for stars in the solar neighbourhood, the authors concluded that the observed spread can be explained by stars coming from different regions of the Galaxy.

Since this effect is not readily explained by plain orbital excursions on epicycles around their birth place (Sellwood & Binney 2002, hereafter SB02), i.e. as an effect of simple heating by the large-scale Galactic structures (arms and bar), another mechanism was invoked: stellar migration (also known as churning). In this paper we will use the definition of SB02; for them, stellar migration is the redistribution of angular momentum for stars produced mainly by their interaction with the large scale non-axisymmetric structures of a galaxy. This process, takes place mainly in the corotation resonance region of a given pattern and has the important characteristic of changing angular momentum of stellar orbits while keeping their orbital eccentricity unchanged.

In Martinez-Medina et al. (2016), we studied exten-

\* Contact e-mail: lamartinez@astro.unam.mx

sively the change of angular momentum induced by the large scale structures of the Galaxy. We found that the bar produces radial migration mainly in the region between 2 and 6 kpc, while the spiral arms dominate for  $R > 6$  kpc. This means that, while in the inner region of the disc the migration is dominated by the joint action of the bar and spiral arms, at outer radii, radial migration is mainly dominated by the spiral arms. We show that the spiral arms are able to imprint their signature in the radial migration with a minimal participation of the bar.

Radial migration (or churning), unlike simple dynamical heating (also known as blurring) that increases the orbital eccentricity, results untrackable since it is not expected to leave kinematic imprints on the spatial origin of the orbits. This would pose a challenge for chemical models because, with increasing flattening due to radial migration, the quantification of the past metallicity gradients (of the stellar population of galaxies) would become increasingly inaccurate.

A lot of work has been devoted to the phenomenon of radial mixing since it was recognized in the 70s. The most recent papers on the subject refer to bars and/or spiral arms as the main mechanisms inducing radial mixing. In the case of the spiral arms, stars close to the corotation region, particularly those with high angular momentum orbits, will suffer radial migration more efficiently due to resonant scatter (e.g. SB02; Roškar et al. 2008, 2012; Schönrich & Binney 2009a,b; Vera-Ciro et al. 2014). Some of the proposals for the mechanisms to produce efficient radial migration (as well as radial displacements) are: fixed corotation long lived spiral arms, usually represented by simple analytical models (e.g. Lépine et al. 2003; Prantzos 2009); transient recurrent spiral arms that change the corotation resonance along large radial extensions of the discs (Schönrich & Binney 2009a; Grand et al. 2012a,b; Loebman et al. 2011); bar and spiral arms resonance overlapping that induces a more efficient redistribution of angular momentum in the disc (Minchev & Famaey 2010; Shevchenko 2011; Brunetti et al. 2011); short-lived transient density peaks originated by interfering spiral patterns (Comarretta & Quillen 2012), and short-lived, recurrent grand design spirals (Athanasoula 2012).

Although the effect of stellar migration on chemical evolution in galaxies is still not quite clear, it is undeniable its impact on the shape of the Milky Way (MW) MDF (Casagrande et al. 2011; Hayden et al. 2015; Loebman et al. 2016; Martinez-Medina et al. 2016). In particular Kubryk et al. (2013) stress the relevance of three factors that contribute to the relation between radial migration and chemical evolution: the strength of the bar or spiral arms (the stronger the structures the larger the effects of radial migration and the larger the effects on the chemical evolution); the duration of the radial migration (the longer, the larger the effects); and the slope of the metallicity curves for a given galaxy (the steeper, the larger the effects). Based on the results of the present work, we concur on the fact that the relation between dynamics (radial migration) and chemistry, depends on the particular galaxy under study.

In this work we have produced a comprehensive orbital study for the MW disc; we employed a novel recipe of chemical tagging as well as an observationally motivated potential model for the MW, that includes the bar and a very detailed three dimensional density based spiral arms potential. Our

study has three purposes, the first one is to produce restrictions for the structural and dynamical parameters of both the bar and the spiral arms. The second, to provide a restriction to the abundance gradient of the disc (at all times and radii), all based on an observable in our Galaxy: the MDF. Lastly, by considering plausible Galactic parameters for the MW, we show that the chemical gradient is nearly conserved at all times in the history of the Galaxy, i.e., neither radial migration nor heating remove the large scale chemical gradient of the MW Galactic disc.

This paper is organised as follows. The galactic model, initial conditions, and methodology are described in Section 2. A study on radial migration, radial heating and the theoretical MDF is presented on Section 3. In Section 4, we present the chemical curves and tagging recipe employed in this work. Our best fit for the dynamical and structural parameters to the MW MDF is shown in Section 5. Restrictions to the chemical gradient in the inner and outer regions of the MW disc are in Section 6. In Section 7, we show the studies of the dynamic effects of the spiral arms and bar imprinted on the MDF. We show the radial reach of migration and heating in Section 8. In Section 9, we present the resulting MDF for populations of different ages. Finally, we present the discussion and conclusions, in Sections 10 and 11, respectively.

## 2 THE GALAXY MODEL

As already described in depth in Martinez-Medina et al. (2016), for this work we have employed an elaborate, three dimensional (although stationary) model, adjusted to the best of recent knowledge of the MW Galaxy structural and dynamical parameters instead of employing the more sophisticated N-body simulations. N-body simulations are not applicable to achieving the goals of this work for the following reasons: a) our model is completely adjustable (contrary to N-body simulations); b) it is considerably faster, adequate to statistical studies like the ones we are presenting in this work; c) because of its nature, this type of models allows us to study in great detail individual stellar orbital behaviour without the known resolution problems of N-body simulations.

The model is composed by an axisymmetric part and a non-axisymmetric part (spiral arms and bar). The axisymmetric potential is based on the potential of Allen & Santillán (1991), that consists of a Miyamoto-Nagai single disc with a vertical height of 250 pc, a spherical bulge, also Miyamoto-Nagai, and a supermassive spherical halo. The spiral arms and the bar are introduced adiabatically by reducing the mass of the disc and the bulge respectively. The Galactic potential is scaled to the Sun's galactocentric distance,  $R_0 = 8.5$  kpc, and the local rotation velocity,  $\Theta_0 = 220$  km s<sup>-1</sup>.

For the spiral arms we employ a model formed by a two-armed 3D density distribution made of individual inhomogeneous oblate spheroids, that we call the PERLAS model (Pichardo et al. 2003). The density is distributed as an exponential decline along the arms. The spheroids act as bricks to construct the spiral arms structure; they are located along a logarithmic spiral locus. PERLAS is completely adjustable (i.e. the width, height, scale lengths, den-

sity fall along the spiral arms and transversal to them, etc.) to better represent the available observations of the spiral arms in the Milky Way. The total mass of the spiral arms taken in these experiments is  $4.28 \times 10^9 M_{\odot}$ , that corresponds to a mass ratio of  $M_{\text{arms}}/M_{\text{disc}} = 0.05$ .

For the bar we have selected a triaxial inhomogeneous ellipsoid built as a the superposition of a large number of homogeneous ellipsoids to achieve a smooth density fall fitted by [Freudenreich \(1998\)](#) from the COBE/DIRBE observations of the Galactic centre. The total mass of the bar is  $1.410^{10} M_{\odot}$ , within the observational limits. Regarding the angular speed, a long list of studies have estimated this parameter concluding that the most likely value lies in the range  $\Omega = 45 - 60 \text{ km s}^{-1} \text{ kpc}^{-1}$ . We adopt the value  $\Omega = 45 \text{ km s}^{-1} \text{ kpc}^{-1}$ , based on the formation of moving groups in the solar neighbourhood.

For all details on the construction and the fit to observations see [Martinez-Medina et al. \(2015, 2016\)](#); [Pichardo et al. \(2003, 2004, 2012\)](#); [Moreno et al. \(2015\)](#); in particular for the present work we have adopted the parameters presented in Section 2 of [Martinez-Medina et al. \(2016\)](#). Brief descriptions of the parameters employed in each simulation are presented across the paper.

### 3 RADIAL MIGRATION, RADIAL HEATING, AND THE SHAPE OF THE MDF

In a disc galaxy, stars orbiting the galactic center exchange angular momentum with non-axisymmetric substructure in the disc. The redistribution of angular momentum in the stellar orbits produces radial migration as well as radial heating, both displace stars from its current galactocentric radius and together encompass what is called radial mixing.

Even when radial migration does not leave a kinematical imprint in the stellar disc, the mechanism can impact some other observables because it can radially displace stars by several kiloparsecs.

Recently there has been found evidence of radial migration in the MW ([Hayden et al. 2015](#)), confirming its ability of shaping the MDF ([Loebman et al. 2016](#); [Martinez-Medina et al. 2016](#)).

In [Martinez-Medina et al. \(2016\)](#), by comparing three galactic models: one with a central bar, one with spiral arms, and one with bar + spiral arms, we found that the change in the skewness of the MDF is mainly driven by the spiral pattern. This means that, through radial migration, the spirals left an imprint in the metallicity distribution of the stellar disc.

#### 3.1 The birth radius as a proxy for metallicity

Since a star preserves information of the state of the ISM at its birth place and epoch, there is a correlation between the birth radius of a star and its metallicity. In order to study the extent of the stellar radial displacements due to radial migration, in [Martinez-Medina et al. \(2016\)](#), we used the birth radius of a star as a proxy for its metallicity. As expected, the initial radii distributions exhibit a change in skewness when going from the inner to the outer disc. Moreover, in the outer disc, we found that the spiral arms are the

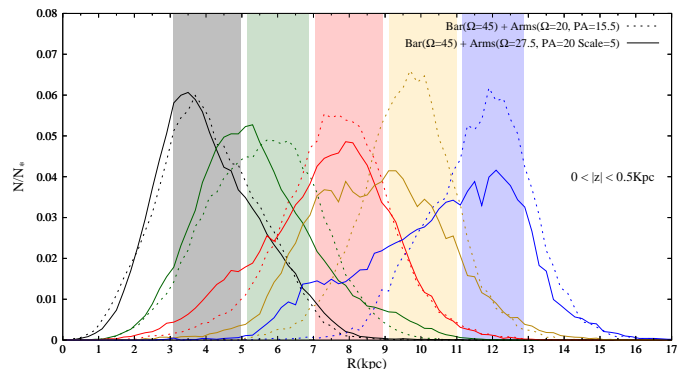


**Figure 1.** Initial galactocentric radii distribution of stars that at the end of the simulation are located within one of the five coloured bins. Each curve corresponds to the closest same-colour shaded bin.  $N$  is the number of stars at a given initial radius and  $N_*$  is the total number of stars that have ended within each coloured bin.

main responsible for shaping the initial radii distributions and hence, the MDFs.

By using the proxy of the birth radius for metallicity, we show how the shape of the MDF depends on the structural parameters of the spiral arms. In Fig 1 we plot the initial radii distribution for two MW models; as indicated in the Figure, the models differ in the structural parameters of the spiral pattern; here we can see the sensibility of the shape of the curves with the amplitude of the spirals and the location of the corotation radius. The purpose of comparing these two models is to show that the initial radii distributions (and hence the MDF) contains information about the structural parameters of the spiral arms.

Although this proxy provides us insight about how the MDF would look like, in the next sections we complement our simulations with a chemical tagging in order to analyse and make a more systematic comparison of the simulated MDFs with those observed in the MW.

## 4 CHEMICAL TAGGING

### 4.1 The Chemical Evolution Model

The evolution of  $[\text{Fe}/\text{H}]$  and Star Formation Rate used in our simulations is obtained from a Chemical Evolution Model for the Galaxy by [Carigi & Peimbert \(2011\)](#). This model was built to match three observational constraints along the Galactic disc: the radial distributions of the surface density of both the total baryonic mass as well as the gas mass, and the O/H radial gradient from H II regions located between 6 and 11 kpc. The O/H gaseous values, determined from recombination lines by [García-Rojas & Esteban \(2007\)](#), were increased due to the correction by dust depletion ([Peimbert & Peimbert 2010](#)).

The main assumptions of the chemical model are: a) the MW disc was formed in an inside-out scenario from primordial accretion with time-scales  $\tau(R) = ((R/\text{kpc}) - 2) \text{ Gyr}$ , where  $R$  is the galactocentric distance; b) for each  $R$ , a double-accretion scenario was assumed, that is, the halo was built with a timescale of  $\tau'(R) = 0.5 \text{ Gyr}$  during the first Gyr and then the disc formed with  $\tau(R)$ , till 13 Gyr (the present

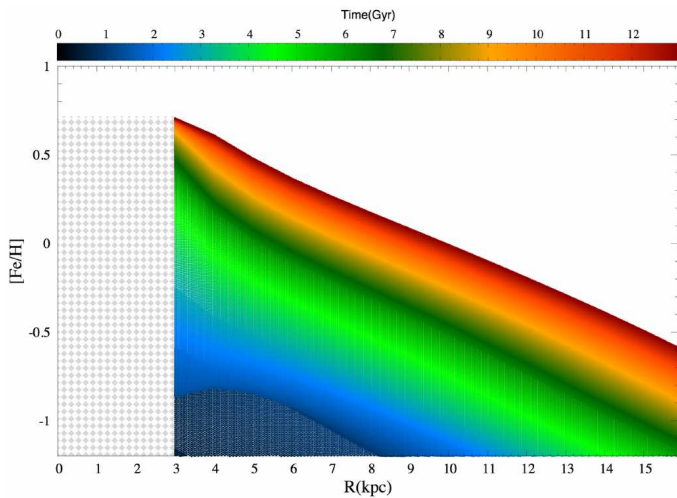


**Figure 2.** [Fe/H] curves for the chemical evolution model of the MW. The color code traces the history of the Galactic disc, from its formation to the present time (13 Gyr).

day); c) the star formation rate was similar to the Kennicutt law (Kennicutt 1998), and its efficiency was five times higher during the halo-forming phase than during the disc-forming phase; d) the initial mass function of Kroupa et al. (1993) was applied in the  $0.08 - 80 M_{\odot}$  range; e) an array of metal-dependent stellar yields for He, C, N, O, Fe, and, Z (all heavy elements) has been used, characterized mainly by stellar yields for massive stars that consider an intermediate mass-loss rate due to stellar winds (see IWY model by Carigi & Peimbert 2011); f) when modeling the chemical evolution of the gas, neither radial flows of gas nor radial migration of stars were considered (note that although the dynamical model feeds of the chemical model, the chemical model does not feed of the dynamical one); g) the chemical evolution model was computed for  $R \geq 3$  kpc, because the Galactic bulge is located in the region  $R \lesssim 3$  kpc and its evolution is quite different to that of the Galactic disc.

As by-products, the model reproduces very well: a) the radial distribution of the stellar mass and the star formation rate; b) the C/H, N/H, O/H, N/O, C/O, and Fe/H gradients; and c) the C/Fe vs Fe/H, O/Fe vs Fe/H, and C/O vs O/H trends shown by stars of different ages in the solar vicinity ( $R \approx 8.5$  kpc) (Carigi & Peimbert 2011; Esteban et al. 2013; Berg et al. 2016).

In Figure 2 we present the original output from the chemical model. The data are shown in an array of metallicity values for galactocentric distances between  $3 \leq R \leq 20$  kpc, going in time from 0 to 13 Gyr (present time), with a high temporal resolution.

As mentioned before, it is uncommon that chemical evolution models provide information of the inner regions of the disc, this due to the lack of observational constraints as well as difficulties in modeling the gaseous component of the Galactic bar and bulge. Such incompleteness leads us to take an assumption for the chemical content of the inner disc,  $R < 3$  kpc, as shown in Figure 3 where an extrapolation towards the center provides us with a complete data set. Let us anticipate that the extrapolation is not arbitrary, it is motivated by the MDFs themselves, as further explained

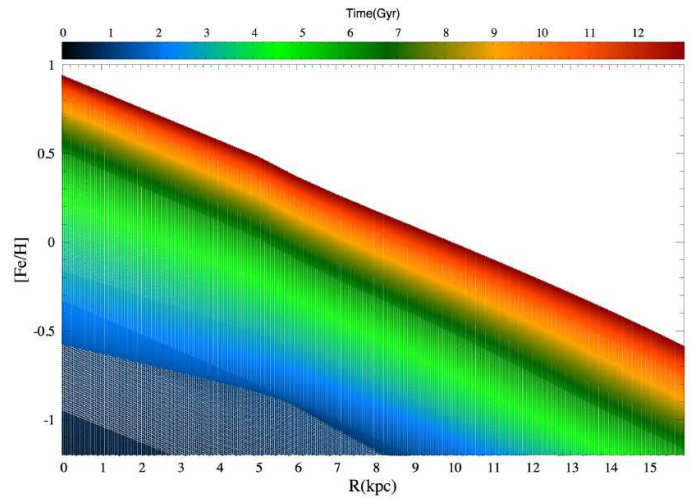


**Figure 3.** [Fe/H] curves extrapolated towards the inner 3 kpc. The color code traces the history of the Galactic disc, from its formation to the present time (13 Gyr).

in Section 6. Also, while this is our initial hypothesis for the chemical gradient, the observed MDFs require a slightly flatter gradient, which we also explain in Section 6.

Before proceeding with the tagging, another key ingredient provided by the chemical evolution model is the Star Formation Rate (SFR) across the disc. Figures 4 and 5 show the assumed SFR for the chemical model employed here. It is important to indicate that, as explained before, the original SFR within the model does not provide information for  $R < 3$  kpc, which means that we need to make a new assumption for the inner disc. Figures 4 and 5 already show the extrapolation of the SFR towards the inner 3 kpc, which was performed as follows.

The entire stellar content of the MW disc is a compendium of a large number of Mono Age Populations (MAPs), covering a very wide range of ages and birth places. Because stars of different ages can coexist at the same epoch, the current distribution of stars in the disc depends on the distribution of individual MAPs, which in turn is dictated by the SFR at each epoch. This means that the present time stellar distribution depends on the SFR at all epochs. On the other hand, the MW model employed here assumes that the stellar distribution of the disc is well characterized by a Miyamoto-Nagai (M-N) density profile, an assumption that works very well in reproducing key observables of the MW (Allen & Santillán 1991).

These two previous arguments can be combined to give the main assumption employed here, i.e., that a M-N density profile represents the current distribution of stars in the disc, and that this distribution is the result of the added contributions of the SFRs at all epochs. To fulfil this constraint, and in order to extrapolate the SFR to  $R < 3$  kpc, we took from the original data not only the SFR at a particular epoch but the sum of the SFRs at all epochs. Next, we fit that sum to a M-N density profile in the center. In this way the fit of the sum give us a functional form that takes into account all the SFRs, and now this functional expression can be used to extrapolate, towards the center, the SFR at any time as shown in Figure 4.

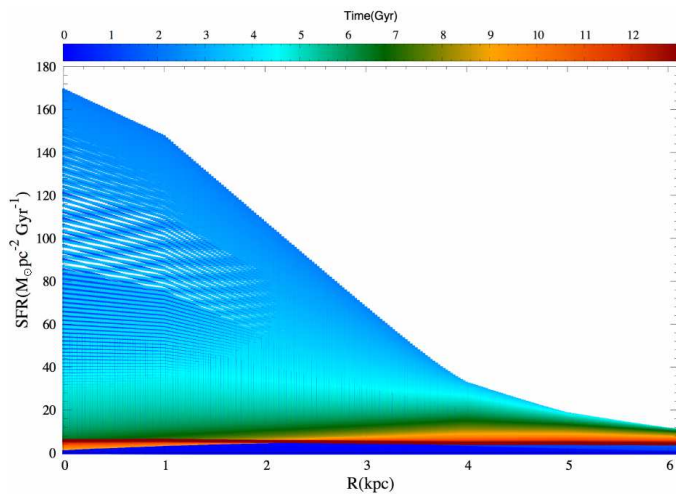


**Figure 4.** SFR in the central region of the disc as a function of galactocentric radius and time, including an extrapolation towards the inner 3 kpc. The color code traces the history of the Galactic disc, from its formation to the present time (13 Gyr).

These two physically motivated extrapolations provide us with complete information about the chemical content (Figure 3) and SFR (Figure 5) of the MW stellar disc. Now we can proceed with the chemical tagging of the particles in our simulations, which consists of the next steps.

The simulation goes from 0 to 13 Gyr and uses one MAP every 20 Myr, for a total of 650 MAPs. The initial conditions for each MAP are constructed as follows: (i) by discretizing a M-N disc profile, (ii) the particle disc is placed inside the axisymmetric potential of the Galactic model and, to avoid spurious transients, we evolve the system for 0.5 Gyr while growing the bar and spirals adiabatically; after which the system is relaxed with the background potential. (iii) Next, to add a MAP to the simulation we take a number of particles proportional to the SFR at every radius and at the epoch represented by each MAP, Figure 5. (iv) Finally, once we have the initial positions, velocities, and the correct number of stars for every MAP, each particle is assigned with the metallicity corresponding at its initial radial position (birth radius) and at that specific epoch (Figure 3).

At the end, our simulations consist of  $1.03 \times 10^8$  stars, with ages between 0 and 13 Gyr, a time in which they evolved dynamically within the galactic potential in the presence of the spiral arms and the bar.

## 5 DEPENDENCE OF THE MDF ON THE MORPHOLOGY OF THE SPIRAL ARMS

In Section 3.1 we have shown how the shape of the initial radii distributions changes with variations of the spiral pattern's features, which lead us to anticipate that the MDFs will also depend on those parameters. By tagging the stars in the simulation with the correct metallicity, according to its birth place and epoch, now we can show that the shape of the MDF contains information about the spiral arms.

From each one of our simulations we take a population of stars with ages between 4 and 4.2 Gyr, and compute the MDFs at different radial bins. In Figure 6 we compare the

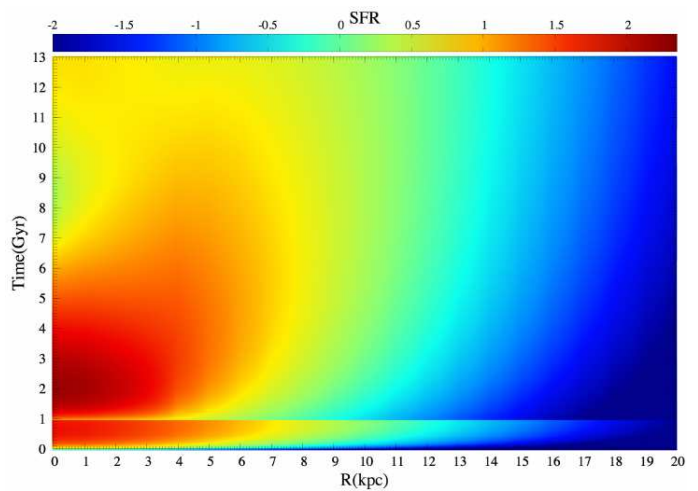


**Figure 5.** SFR, along the entire disc, as a function of galactocentric radius and time, including an extrapolation towards the inner 3 kpc.

MDF of several galactic models that differ in the structural parameters of the spiral arms. Top panel shows how the shape of the MDF depends on the scale radius of the spirals, i.e., the mass concentration of the pattern. A less concentrated pattern means more arm's mass at outer radii, which in turn means that stars at those locations will experience a larger gravitational attraction during their encounters with the spirals. Because in its orbital motion the acceleration towards the arms will be larger, less concentrated arms will induce a greater exchange of angular momentum and hence, a more significant radial migration. In the top panel of Figure 6 we can see that the MDF is almost unaffected in the three inner radial bins. For the rest of the bins the distributions are wider and their peaks are lower for the less concentrated spirals, which means that the radial mixing is larger. Notice that the radial mixing due to less concentrated arms can be so efficient that, for example, the MDF corresponding to the red bin ( $11 < R < 13$  kpc) reverse its skewness compared to more concentrated spiral arms. Also, for the yellow bin ( $13 < R < 15$  kpc), there is more migration of stars that come from the inner disc. This is reflected on a MDF with an inner tail of higher amplitude, which increases the asymmetry of the curve.

The most important dynamical parameter inducing migration in the outer disc is the spiral arm pattern speed. This happens because the value of the pattern speed determines the position of the corotation radius, and radial migration occurs when the stars exchange angular momentum with the spiral arms around corotation. The second panel of Figure 6 shows the comparison of two models that differ in the spiral pattern speed. When changing  $\Omega$  from 20 to 27.5  $\text{km s}^{-1} \text{kpc}^{-1}$  the corotation radius moves from 10.9 to 8 kpc. The most affected MDF is the red one ( $11 < R < 13$  kpc), its skewness is reversed again and its inner tail raises, which means that this radial bin has more contribution of stars that come from the inner disc. The other MDF that changes significantly is the green one ( $9 < R < 11$  kpc), being shifted towards higher metallicities.

The other important parameter of the spiral arms, that

determines the amount of angular momentum that the pattern can exchange, is the pitch angle. An increase of the pitch angle increases the gravitational attraction of the spiral perturbation on the stars along their orbital direction. By accelerating stars along their rotational motion, they gain or lose more angular momentum, moving to larger or smaller radii. The third panel of Figure 6 shows the comparison of two models that differ in the pitch angle of the spiral arms. By changing slightly the pitch angle, from  $15.5^\circ$  to  $20^\circ$ , we can see that the most affected MDFs are those of the two outer radial bins ( $11 < R < 13$  kpc and  $13 < R < 15$  kpc). The inner tail for both distributions raises enough to see that these radial bins are getting more contribution of metal rich stars that were born at inner radii, increasing the skewness of the curves.

Finally, the bottom panel of Figure 6 shows the differences in the MDFs when we change all those three important structural parameters of the spiral arms: scale radius, pattern speed, and pitch angle. The differences between both models are significant, showing that the shape of the MDF contains information about the spiral pattern as well as of the dynamical evolution of the stellar disc.

## 6 CONSTRAINING THE METALLICITY GRADIENT IN THE INNER AND OUTER MW DISC

As mentioned in Section 4, chemical evolution models for the MW disc do not include, in general, information within the inner 3 kpc. This is due to the difficulty to separate the different Galactic components that overlap in the center of the Galaxy, but also due to the lack of observational data to constrain a chemical model in the central region.

A common assumption to overcome this problem is to take the value of the chemical abundance at  $R = 3$  kpc, and assign it for all the inner region ( $R < 3$ ) kpc, i.e., the metallicity gradient will be zero in the inner 3 kpc. Although constant chemical content in the center of the Galaxy is a first guess, it probably is not realistic. From a dynamical point of view, it is known that the stars can displace radially by several kpc, driving a chemical “contamination” at all galactocentric distances (i.e. different abundances from those of the birth radius).

From our simulations we notice that the most inner radial bin considered ( $3 < R < 5$  kpc) receives a significant number of stars born at  $R < 3$  kpc (see for example Fig. 1). If all the stars born at  $R < 3$  kpc share the same metallicity (zero metallicity gradient assumed), they would contaminate the stellar disc with the same metallicity when they displace to outer radii. This would be reflected in our two inner MDFs ( $3 < R < 5$  kpc and  $5 < R < 7$  kpc) by producing a huge spike at a specific  $[\text{Fe}/\text{H}]$  value. This would produce unrealistic distribution curves that show us that assuming zero metallicity gradient in the inner disc is unsuitable. In other words, the assumed chemical content in the inner 3 kpc will have an important impact on the observables at  $R > 3$  kpc. Here we propose a fit to the MDFs of the MW as a method to constrain the chemical evolution models toward the center of the disc.

Noticing that close to the plane, the two inner MDFs reported by Hayden et al. (2015, Fig. 5) overlap, we tried

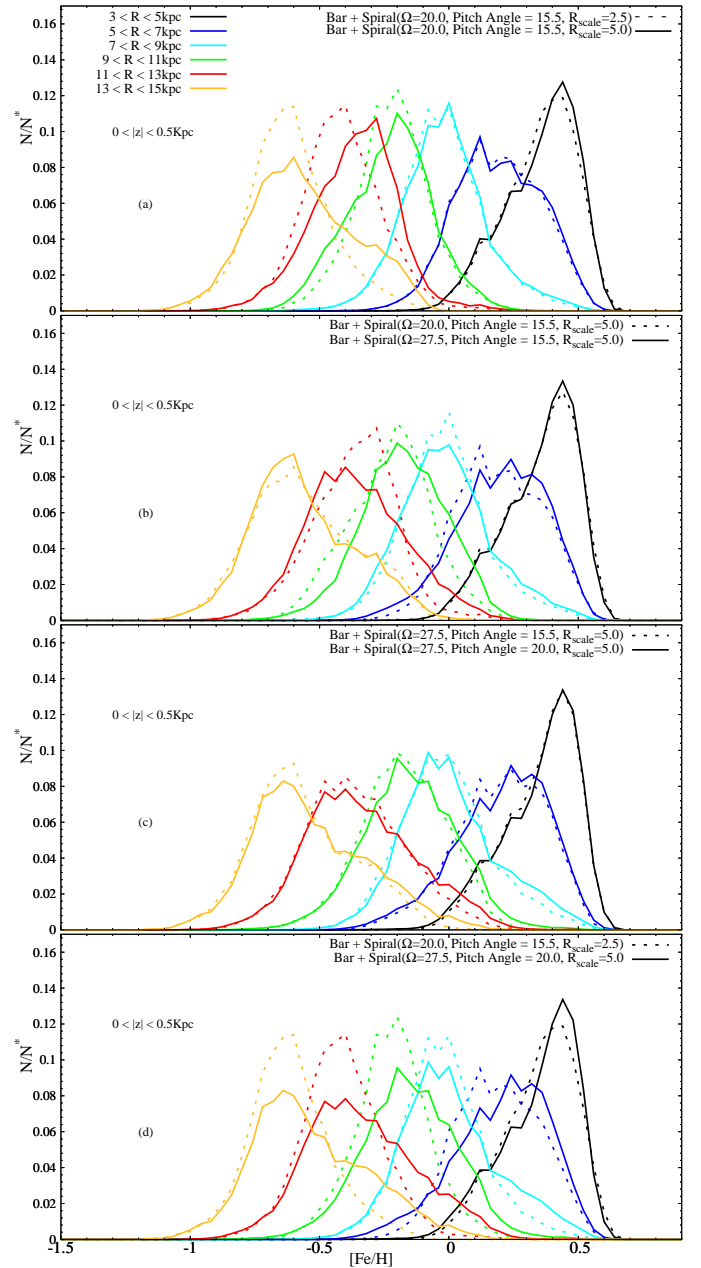


**Figure 6.** MDF as a function of the galactocentric radius for different characteristics of the spiral arms for a population of stars between 4 and 4.2 Gyr. The panels show how the shape of the MDF depends on (a) the scale radius of the spirals, (b) the pattern speed, (c) the pitch angle, and (d) the combination of those three parameters.

to obtain similar MDFs from our simulations by changing the gradient of the chemistry curves, at  $R < 3$  kpc, in order to avoid the unrealistic spike in the inner MDFs, tuning the gradient to obtain a similar degree of overlapping, as is observed. Our best fit to the observed MDFs provide us a chemical curve along the entire disc that includes the prediction at inner radii in Figure 3.

Moreover, since the observed MDFs peak at high metallicities in the inner Galaxy, then peak approximately at a

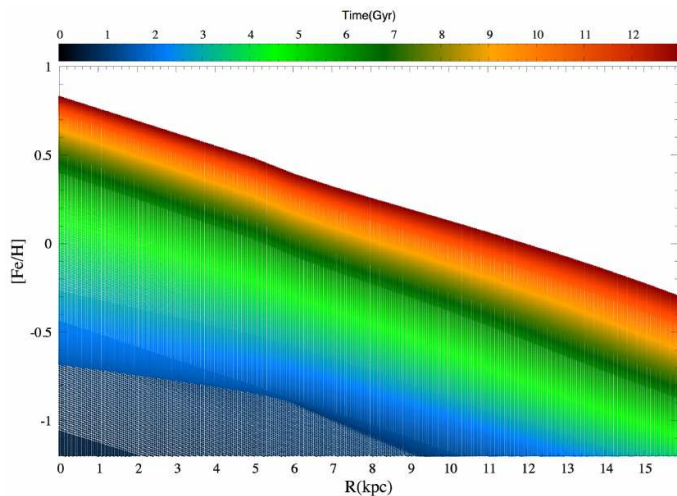


**Figure 7.** [Fe/H] curves for the chemical evolution model of the MW, including the extrapolation towards the inner 3kpc and the modified gradients to better reproduce the resulting MDFs. The color code traces the history of the Galactic disc, from its formation to the present time (at 13 Gyr).

solar value in the solar neighbourhood, and peak at lower metallicities in the outer disc, the observed MDFs also show the radial metallicity gradient across the disc, which puts additional constraints on our simulation. When using the chemical gradient as presented in Figure 3, we find that the stars lie between  $-0.65 < [\text{Fe}/\text{H}] < 0.65$ , while the vast majority of stars in the sample presented by Hayden et al. (2015) have values of [Fe/H] between  $-0.5$  and  $0.5$ . This suggests that the actual chemical gradient of the MW is slightly flatter than the  $-0.102 \text{ dex kpc}^{-1}$  presented in Figure 3. By flattening the chemical gradient by 22% to  $-0.080 \text{ dex kpc}^{-1}$ , we reproduce the range observed by Hayden et al. This means that, by confining the peaks of the simulated MDFs to the reported values, we improve the chemical evolution model via the restriction of the radial gradient across the disc.

Figure 7 shows the final chemical model obtained by (i) extrapolating the chemical content towards the inner disc (in order to overlap the two inner MDFs, without the unrealistic spike), and (ii) confining of the MDF peaks between  $-0.5 < [\text{Fe}/\text{H}] < 0.5$ .

## 7 STELLAR DYNAMICS IMPRINTED IN THE METALLICITY DISTRIBUTION

In this work we propose an analysis of the MDFs as a method to obtain information on the structure and dynamics that shape the spiral arms and bar of galaxies. We apply this to the Milky Way, where the MDFs have been observed in great detail.

As we have mentioned, the interactions of the stars with the non-axisymmetric structures in the disc can modify the stellar orbits either by heating or by radial migration. Heating occurs when the orbital eccentricity increases, and can be quantified directly from the kinematics of the stars; in this case, the velocity dispersion can provide a good idea of the dynamical evolution of a given star field; e.g. it is

**Table 1.** Parameters of the non-axisymmetric Galactic components.

Parameter	Value
<i>Triaxial ellipsoidal Bar</i>	
Major Semi-Axis	3.5 kpc
Scale Lengths	1.7, 0.64, 0.44 kpc
Axial Ratios	0.64/1.7, 0.44/1.7
Mass	$1.4 \times 10^{10} M_{\odot}$
Pattern Speed ( $\Omega_B$ )	$45 \text{ km s}^{-1} \text{ kpc}^{-1}$
<i>Spiral Arms</i>	
Number of spiral arms	2
Pitch Angle ( $i$ )	$20^{\circ}$
Radial Scale Length ( $H_{\star}$ )	5 kpc
$M_{\text{arms}}/M_{\text{disc}}$	0.05
Mass	$4.28 \times 10^9 M_{\odot}$
Pattern Speed ( $\Omega_S$ )	$27.5 \text{ km s}^{-1} \text{ kpc}^{-1}$

known that the age and velocity dispersion of stars are correlated (see for example Holmberg et al. 2009; Roškar et al. 2013; Gerssen & Shapiro Griffin 2012; Seabroke & Gilmore 2007; Mayor 1974; Carlberg et al. 1985). On the other hand, when migration takes place the mean galactocentric distance of the star changes significantly, but its orbital eccentricity does not; this means that, unlike with heating, migration cannot be revealed through stellar kinematics; instead, recent observations and numerical simulations have shown that this dynamical process can be revealed through the MDFs.

Since the shapes of the MDFs measure displacements of stars away from their birth radius, they capture both processes, heating as well as migration. We argue that the shape of the MDF not only tells us whether the stellar disc experienced migration, but also contains specific information about the structure that triggered such migration. We have come up with this conclusion by (i) finding that the spiral arms are the ones that determine the sign in the skewness of the MDFs (Martinez-Medina et al. 2016), and (ii) showing how the shapes of the MDFs are sensitive to the structural parameters of the spiral pattern (see Section 5).

In Figure 8 we present the results of a simulation that includes the central bar and the spiral pattern (see Table 1 for the specific parameters employed). In this figure, we have reproduced closely characteristics observed in the MDFs of the MW, as reported by Hayden et al. (2015), such as, (i) the negative skewness in the inner disc (with tails that extend to low metallicities), which is reversed at the outer disc (with tails that extend to high metallicities); (ii) there is an evident radial metallicity gradient across the disc in spite of the significant radial mixing; and (iii) the peaks of the MDFs are confined within the interval  $-0.5 < [\text{Fe}/\text{H}] < 0.5$ , which provides us the value of the radial gradient.

Heretofore, the analysis of the MDF gave us important clues on the chemical and dynamical evolution of the stellar disc. A more detailed insight of what is happening in the disc can also be obtained by studying the plane [Fe/H] vs.  $R$ . Figure 9 shows the metallicity distribution across the disc for a population of stars with ages between 4.6 and 5.6 Gyr, in a MW model with the parameters for the bar and spiral arms given on Table 1. Every point in the plot represents a

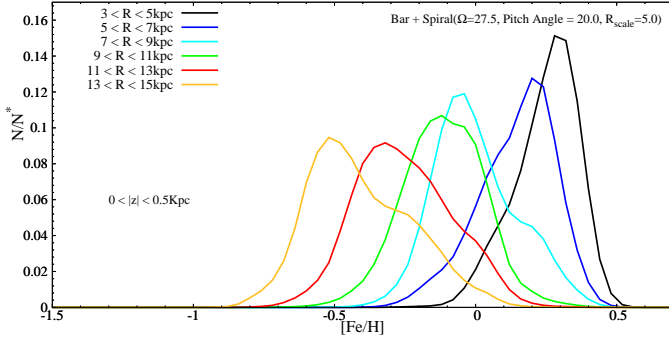


**Figure 8.** MDFs as a function of galactocentric radius for a Galactic model with the parameters of Table 1 and iron abundance gradients from Figure 7, for stars with ages between 4.6 and 5.6 Gyr.

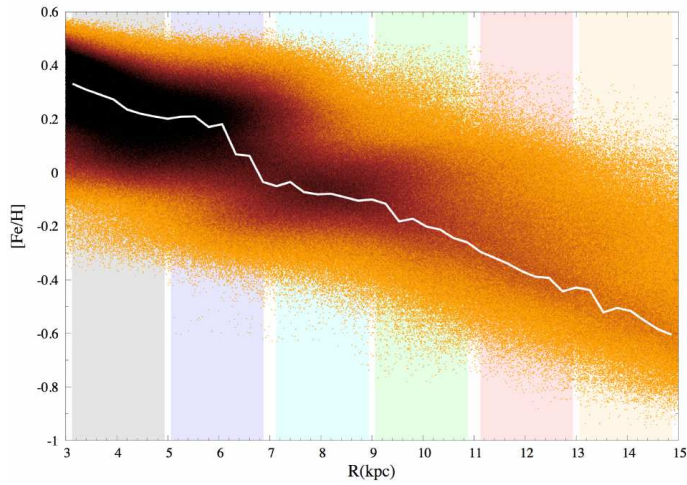


**Figure 9.** Distribution of stars in the plane  $[\text{Fe}/\text{H}]$  vs. Radius corresponding to the simulation of Figure 8, and stellar ages between 4.6 and 5.6 Gyr. The colour code indicates density of stars, while the solid white line is the mode of the  $[\text{Fe}/\text{H}]$  values at every radius. The background coloured bands are set as reference to compare with the same color MDFs in Figure 8.

star at its current galactocentric radius and its metallicity, the color coding indicates the density of stars. In Figure 9 we can see in more detail the extended tails that appear in the MDFs from previous figures; for instance, at the inner radial bins the peak in density of stars is not centered in the middle of the orange band, but a little shifted to the top; on the other hand, in the outer radial bins, the peak in density is located at low metallicities, near the bottom of the orange band, with an important number of stars at high metallicities. Also, while the MDF tells us the radial bin to which the star belongs, the  $[\text{Fe}/\text{H}]$  vs.  $R$  plane provides its exact location within the bin. For example, stars with high metallicity that were born at the inner disc but now are located in the outer radial bin ( $13 < R < 15$  kpc) did not migrate to only reach the inner boundary of that bin, but as Figure 9 shows, they migrated also to the outer boundary of the bin.

The most prominent features in Figure 9 are the two

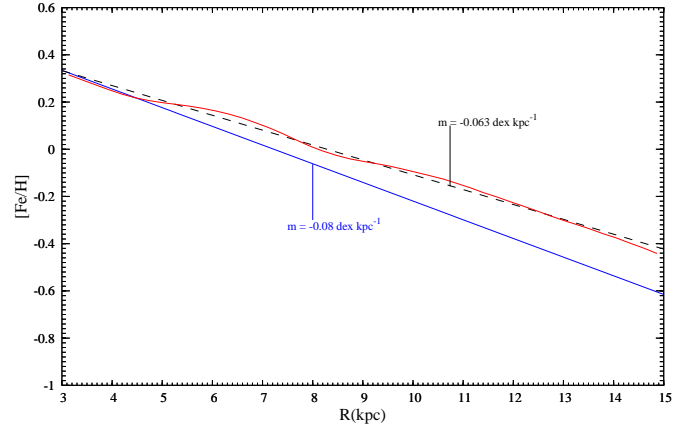


**Figure 10.** The mean of the  $[\text{Fe}/\text{H}]$  values (red line) for the data plotted in Figure 9. The blue line indicates a linear fit to the iron abundance of the stellar population at its birth epoch. Black dashed line is a linear fit to the mean iron abundance at the present time.

overdensities at  $R = 4.7$  kpc,  $[\text{Fe}/\text{H}] = 0.25$  and at  $R = 8$  kpc,  $[\text{Fe}/\text{H}] = -0.1$ . The break between these two overdensities marks the transition between the influence of the bar to the influence of the spiral pattern, i.e. the inner overdensity is composed by stars that have been strongly affected by the corotation of the bar, while the outer one is composed by stars that have been strongly affected by the corotation of the spiral pattern. This behavior is studied in depth in [Martinez-Medina et al. \(2016\)](#).

Notice that Figure 9 shows the density of stars in the  $[\text{Fe}/\text{H}]$  vs.  $R$  plane, and hence the mode of the data (white curve, and hence the mode of the data) indicates directly the density peaks. However, to quantify the metallicity gradients for this stellar population, Figure 10 shows the mean of  $[\text{Fe}/\text{H}]$  as a function of  $R$ . The blue line corresponds to the initial metallicity gradient, which is a linear fit to the iron abundance of the population at its birth epoch. The red curve is the mean of the data plotted in Figure 9, while the black dashed line is a linear fit to the red curve, and hence, the metallicity gradient of the present stellar population. It is clear that the metallicity gradient evolved with time, but still the two slopes are not very different. It is worth noticing that at the present time the stellar population exhibits a clear metallicity gradient in spite of the important radial migration and heating in the disc. This means that the presence of important radial migration does not imply necessarily a substantial flattening of the metallicity gradient (see also [Schönrich & McMillan \(2017\)](#) for a similar conclusion).

## 7.1 Metallicity gradients away from the Galactic plane

Because stars with small vertical oscillations remain close to the plane, having more interaction with the non-axisymmetric structures on the disc, they are the most efficiently affected by radial migration. However, stars with large vertical excursions or large vertical velocities still can experience radial displacements, that could contribute to a changing metallicity gradient when the altitude away from

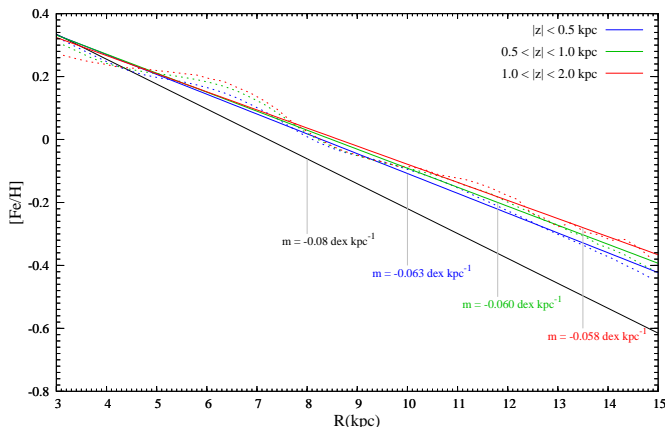


**Figure 11.** Radial metallicity gradients, for a stellar population with average age of 5Gyr, at different vertical distances from the plane. The black line indicates the initial gradient for the entire population regardless of  $z$ .

the plane increases, as is the case for the solar neighborhood (Nordström et al. 2004; Boeche et al. 2013, 2014).

In this section we go beyond the thin disc to compare the metallicity gradient obtained at different ranges of  $z$ . As mentioned above, from our simulation we took a population of stars with ages between 4.6 and 5.6 Gyr. Figure 11 shows the mean of the  $[\text{Fe}/\text{H}]$  distribution as a function of  $R$  for three ranges of  $z$  (dashed lines). The solid lines indicate a linear fit for each one of these mean curves, while the black line is the initial  $[\text{Fe}/\text{H}]$  gradient of the entire population. The first thing to notice is that the final metallicity gradient becomes less steep with increasing height. However, although the tendency is clear, the differences between the three gradients is rather small.

We interpret the trend shown in Figure 11 not as a direct consequence of radial migration, but as a result of the biased nature of the mechanism. In other words, because the stellar density of the disc decreases with radius, more migrators will arrive, at a given radial position, from the inner disc than from the outer disc; this means that at that radial position the excess of metal-rich stars will contribute positively to the metallicity gradient, making it less steep. The effect becomes evident with increasing radius and even more with increasing height, where the number of stars is small. Kawata et al. (2017) obtain a similar result, observing that this bias leads to a positive vertical metallicity gradient.

The bias in the radial migration mechanism, producing more outward than inward migrators, is also reflected in the MDFs. Figure 12 shows the MDFs across the disc, going in  $|z|$  from 0 to 2 kpc. Notice that when  $|z|$  increases, the position of the peaks and the shape of the curves remain nearly unchanged, except for the two outer radial bins (red and yellow distributions). The peak of the outmost MDF shifts to higher metallicities as the height increases, just reflecting the fact that at those radial positions and altitudes there are still stars arriving from the inner disc, but the density has dropped to a point that there are almost no stars coming from the outer disc.

At the end, although this bias affects mainly the outer regions of the disc and becomes more evident at high alti-

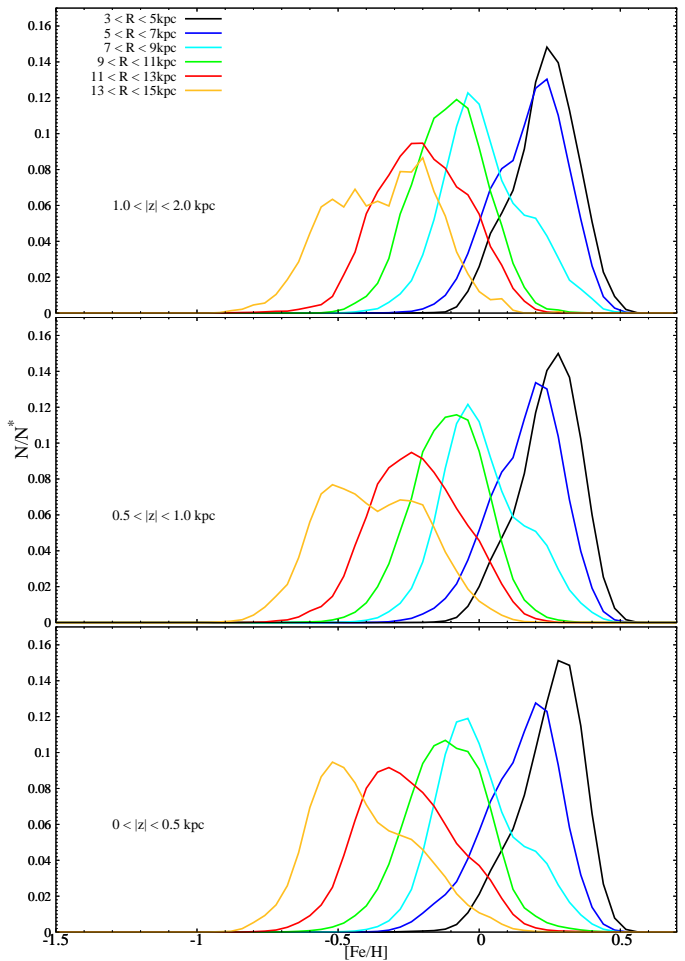


**Figure 12.** MDFs as a function of galactocentric radius, at different heights away from the plane, for stars with ages between 4.6 and 5.6 Gyr. The computations were performed using a Galactic model with the parameters of Table 1 and iron abundance gradients from Figure 7.

tudes, Figure 11 shows that a metallicity gradient is clear and differs just slightly when going from the thin to the thick disc.

## 8 THE RADIAL REACH OF MIGRATION AND HEATING

In the previous sections we have seen how the presence of spiral arms or a bar in a disc galaxy displace stars radially, with an important fraction of them being moved away from their birth radius. As already mentioned, the displacements occur because the stars gain or lose angular momentum when interacting with the pattern (spirals or bar). For example, in the case of spiral arms, a star can be orbiting either in front of the pattern or behind it. If the star is ahead of the arm, the overdensity of the pattern will pull the star backwards, diminishing its angular momentum, which will cause the star to move to inner radii. Similarly, if the star is located behind the pattern, it will be pulled forward, which increases its angular momentum, moving the star to larger

**Table 2.** Radial displacements across the disc.

$R_{final}$ (kpc)	$\langle \Delta R \rangle$ (kpc)	$\sigma_{\Delta R}$ (kpc)
1	-0.43	0.85
2	-0.28	1.07
3	-0.22	1.25
4	-0.29	1.36
5	0.08	1.4
6	0.57	1.7
7	0.64	1.9
8	0.55	1.7
8.5	0.68	1.57
9	0.9	1.57
10	1.24	1.88
11	1.4	2
12	1.43	2.1

radii. These two scenarios mean that, at any given radius, the spirals or the bar can induce radial displacements in both directions.

In this section we quantify the extension of the radial displacements in the orbits of stars. Figure 13 shows the difference between the current position of every star and its birth radius,  $\Delta R = R_{final} - R_{birth}$ , as a function of its current galactocentric position  $R_{final}$ , for a population with ages between 4.6 and 5.6 Gyr. Notice that during their lifetime, after evolving in the Galactic potential, an important fraction of stars end up several kpcs away from their birth radius, with radial excursions either to larger or inner radii. To identify any trend in the displacements, the red solid line in Figure 13 indicates the mean of the  $\Delta R$  values as a function of  $R_{final}$ . Notice that  $\langle \Delta R \rangle$  is negative for the first 5 kpc, indicating a tendency to move from the outer to the inner disc. Meanwhile for  $R_{final} > 5$  kpc the trend is that, in average, the stars were born at inner radii, and were displaced outwards to their current position.

In the particular case of the solar circle ( $R_0 = 8.5$  kpc) the average displacement is  $\langle \Delta R \rangle_0 \approx 0.68$  kpc. However, this value is just the average, and the fraction of stars that were born at radii considerably smaller and end up at the solar radius can be important. The dashed lines in Figure 13 indicate the dispersion of the data,  $\pm \sigma_{\Delta R}$  around the mean, as a function of  $R_{final}$ . At the solar circle  $\sigma_{\Delta R} \approx 1.57$  kpc, which added to  $\langle \Delta R \rangle_0$  means that stars within  $1\sigma_{\Delta R}$  reached the solar circle from galactocentric positions  $6.25 < R_{birth} < 9.39$  kpc. Table 2 shows the same analysis for different galactocentric distances across the disc. Within a  $1\sigma_{\Delta R}$  dispersion, stars with  $R_{final} > 6$  kpc can be displaced for more than 2 kpc. Figure 13 also shows that the radial displacements for  $R_{final} > 6$  kpc can be considerably large.

### 8.1 The Birth Place of the Sun

We have seen that stars can undergo radial displacements of several kiloparsecs, meaning that for an important fraction of stars their birth radius is very different from their current galactocentric distance. Moreover, during its evolution in the galactic potential, the orbital elements of a star can change rapidly, erasing all kinematic hints about their birth radius. However, as we already mentioned, an indication of whether

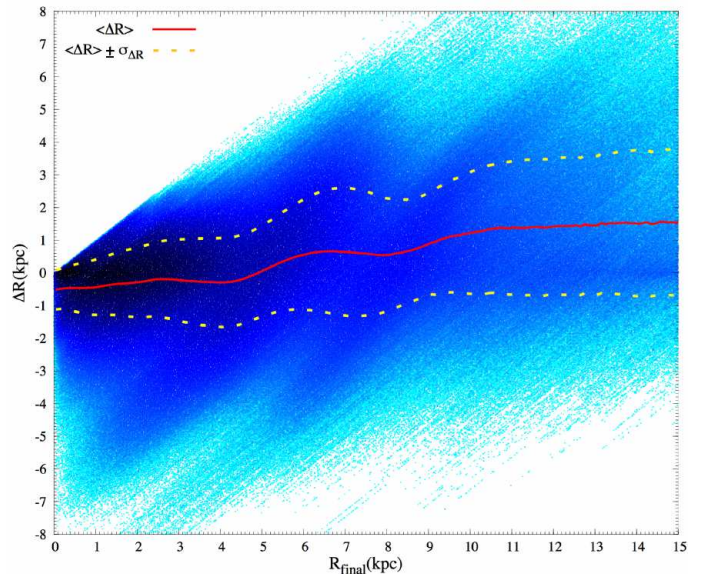


**Figure 13.** Difference between the current position of every star and its birth radius,  $\Delta R = R_{final} - R_{birth}$ , as a function of its current galactocentric position  $R_{final}$ , for a population with ages between 4.6 and 5.6 Gyr. The color coding indicates the density of stars in logarithmic scale. The red solid line shows the mean of the  $\Delta R$  values as a function of  $R_{final}$ . The dashed lines indicate the dispersion of the data,  $\pm \sigma_{\Delta R}$  around the mean, as a function of  $R_{final}$ .

the stars have migrated or not, and how far are they from their birth radius, is their chemical content.

For the particular case of the Sun, it has been found that it is more metal rich than the majority of solar age stars in the solar neighbourhood. The high metallicity of the Sun can be explained assuming that it migrated outwards, from its birth, place to its current galactocentric distance (e.g. Wielen et al. 1996; Holmberg et al. 2009; Nieva & Przybilla 2012). Different results, based only on orbital dynamics, show a possible migration inwards, from its birth place, to its current position (Martínez-Barbosa et al. 2015). In this section we discuss plausible sources of discrepancy with chemical determinations and with the results in this work.

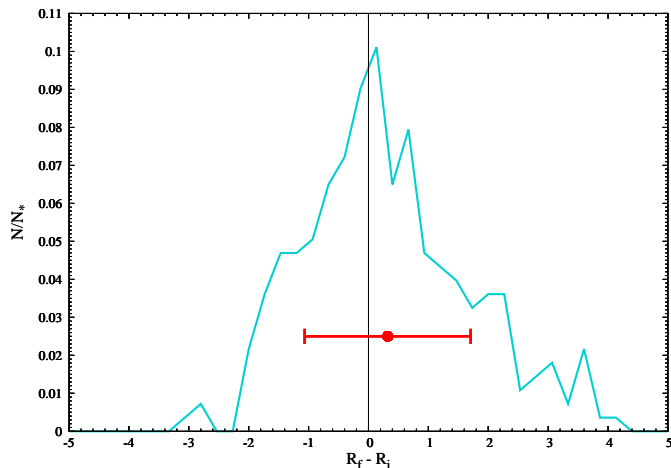
Taking advantage of the large number of particles in our simulations, we test the plausibility of a migration scenario for the Sun. From the simulation we select the stars with orbital properties similar to the current ones of the Sun, i.e. position, velocity with respect to the local standard of rest (LSR), and age. Then, for those stars that fulfill the selection criteria, we trace back their birth radii.

For the present-day galactocentric distance of the Sun, its altitude above the galactic plane, and its velocities, we take the values listed in Table 3. The velocities  $(U, V, W)_\odot$  (Schönrich et al. 2010) are taken with respect to the LSR, that in our galactic model has the value  $V_{LSR} = 220$  km  $s^{-1}$ . The standard deviation in each orbital parameter corresponds to the uncertainties in each reported value.

As the mean age reported for the Sun is 4.6 Gyr, we selected those stars with ages between 4.4 and 4.8 Gyr. When looking in our sample for stars with orbital parameters within the restrictions presented in Table 3, we found none of our  $10^8$  stars met the criteria. For this reason, from

**Table 3.** Sun’s orbital parameters.

Coordinate	value		
$R_{\odot}$	8.5	$\pm$	0.5 kpc
$z_{\odot}$	0.02	$\pm$	0.005 kpc
U	11.1	$\pm$	1.23 km s <sup>-1</sup>
V	12.24	$\pm$	2.1 km s <sup>-1</sup>
W	7.25	$\pm$	0.62 km s <sup>-1</sup>

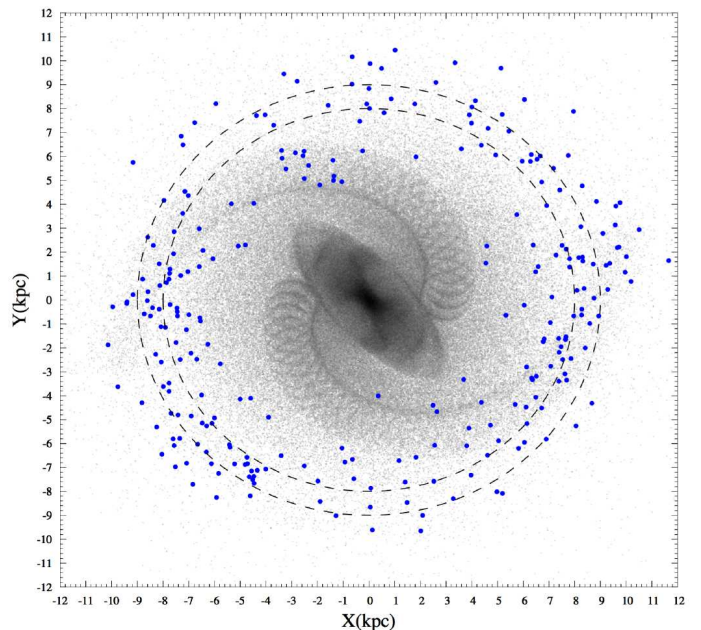

**Figure 14.** Distribution of radial displacements of the stars that currently share the age and orbital parameters of the Sun. The vertical line divides inwards from outwards migrators, while the red dot represents the 0.32 kpc average, with a 1.38 kpc dispersion of the sample.

the stars with those ages and radii, we selected the ones with altitude above the plane  $z = z_{\odot} \pm 3\sigma_z$ , and velocities  $(U, V, W) = (U_{\odot} \pm 3\sigma_U, V_{\odot} \pm 3\sigma_V, W_{\odot} \pm 3\sigma_W)$ , where the standard deviation  $\sigma$  was taken as the uncertainty in each reported value. With this relaxed criteria we found only 277 stars that fulfill all our restrictions; the scarcity of these particles is not surprising given the amount of phase space volume available. The result of this selection procedure is shown in Figures 14 and 15.

Figure 14 shows the distribution of radial displacements of our Sun-like stars. The displacements are centered at  $R_f - R_i = 0.32$ , with a dispersion of 1.38 kpc; some stars migrating as much as 4 kpc outwards or 3 kpc inwards, with 56% of our sample moving outwards and 44% moving inwards.

Figure 15 shows the birth place on the galactic plane as well as the configuration of the bar and spirals 4.6 Gyr ago, for the stars that fulfill our selection criteria. Notice that the distribution of stars is not axisymmetric, with most stars being born in the arm or just behind it, and very few being born ahead of the spiral arms.

The previous analysis shows plausible scenarios that place the birth radius of the Sun away from its current position, showing, with a high probability, that the Sun was born at a galactocentric distance of  $R_{\odot} = 8.18 \pm 1.38$  kpc. However, the fact that we find hundreds of strongly migrating stars that mimic closely the current solar parame-


**Figure 15.** Position in the galactic plane for stars that fulfilled our selection criteria. Blue dots indicate their birth place, while the gray color gradient shows the configuration of the bar and spirals at that moment. The ring indicates the current solar radius of  $8.5 \pm 0.5$  kpc

ters, shows that the study of radial migration will not be able to accurately constraint the birth place of the Sun; this is true for our approximation to the Galaxy, as well as it would be to any model of the Galaxy that is more complete (complex) than ours. Also, the likelihood of a strong migration would pose serious difficulties for instance, to the possibility of finding any solar siblings since the long excursion through the Galaxy, would exert a strong shear that would have probably dissociated the Sun’s birth cluster rapidly.

Other pure dynamical based works find a tendency for the Sun to have originated on the outer parts of the Galaxy (Martínez-Barbosa et al. 2015), this is not compatible with what is found chemically. However, in that work, although their conclusions indicate that the Sun comes from the outer parts of the Galaxy, their figures cannot rule out the possibility that it could have come from the inner region. Still, some (small) discrepancy remains on the percentage of migrators, relative to what it is obtained in this work; this could be probably due to the simplified potential model they employ or to the fact that integrating backwards in time in chaotic regions (e.g. near overlapping resonances), may introduce systematic errors.

Considering that it is unlikely that the Sun was formed near its current galactocentric position, it may be inaccurate to consider the Sun as representative of the chemical abundances in the solar neighborhood; this was also noticed by Nieva & Przybilla (2012) with chemical studies of nearby B stars. Edvardsson et al. (1993) and Wielen et al. (1996) also find that the metallicity of the Sun suggests that it was formed in the inner disk of the Galaxy.

A better way to estimate the birth radius of the Sun, is to combine the dynamical information with what can be obtained by comparing its chemical composition with that

of young objects (HII regions, B stars, etc.) and, using what is known of the metallicity gradient and chemical evolution of the MW, to determine the likely origin of the Sun. In our chemical model, the solar metallicity, 4.6 Gyr ago, was observed at a galactocentric distance of 7.7 kpc, and once including reasonable errors for the Sun’s chemical abundance, as well as errors in the determination of the chemical gradient and evolution of the MW, this translates to:  $7.7 \pm 1$  kpc; combining this with our dynamical determination we find that the Sun was likely to have formed at a galactocentric distance of  $7.9 \pm 0.8$  kpc.

## 9 THE MDF FOR DIFFERENT AGE POPULATIONS

Up to this point we have shown how the MDF looks for a given MAP, or more precisely, for stars within a narrow age range. For example, the MDFs in Figure 8 reveal a metallicity gradient across the disc, with long extended tails producing asymmetric curves, and with peak metallicity values constrained between  $-0.5 < [\text{Fe}/\text{H}] < 0.5$ . But how do they look like for younger or older stars? i.e., how are the MDFs be for different stellar ages?

As described above, our simulations are an extensive compendium of mono-age populations, with number of stars and distribution across the disc given by the SFR at their birth epoch. Also, as we applied a chemical tagging according to the data in Figure 7, we can compute the MDFs for any age.

Figure 16 shows the MDFs for three narrow age intervals in the simulation, going from very young to very old stars. In the top panel, for the youngest stars, the MDFs are narrow with high amplitude, meaning that, for most of the stars, the metallicity is the one expected at that radial position. In other words, this is an indication that the current galactocentric distance of the star is not very different from its birth radius.

In the middle panel of Figure 16, for stars of intermediate age, the MDFs are clearly different from the previous case, specially for the outer radial bins. First notice that, as a consequence of the lower metal content of the disc at earlier epochs, all the curves are shifted toward lower values of  $[\text{Fe}/\text{H}]$ . They are wider, have decreased in amplitude, and the asymmetry is more evident. These features are the signatures of an effective radial mixing of the stellar disc, particularly one driven by radial migration, that we know now is the responsible for the extended tails and opposite skewness (when going from the inner to the outer disc) in the MDFs.

The bottom panel of Figure 16 shows the MDFs for very old stars. As in the previous case, the curves are shifted toward even lower values of  $[\text{Fe}/\text{H}]$ ; the curves have smaller amplitudes and are wider compared to the previous cases. Note how for the inner radial bins, the internal tail of the curve extends toward low metallicities, while for the outer radial bins, the external tail of the curves extends toward large metallicity values. The extension of the tails and the pronounced asymmetry in the MDFs of very old stars is clear evidence of significant radial mixing, which is what one would expect from an old, dynamically more evolved population.

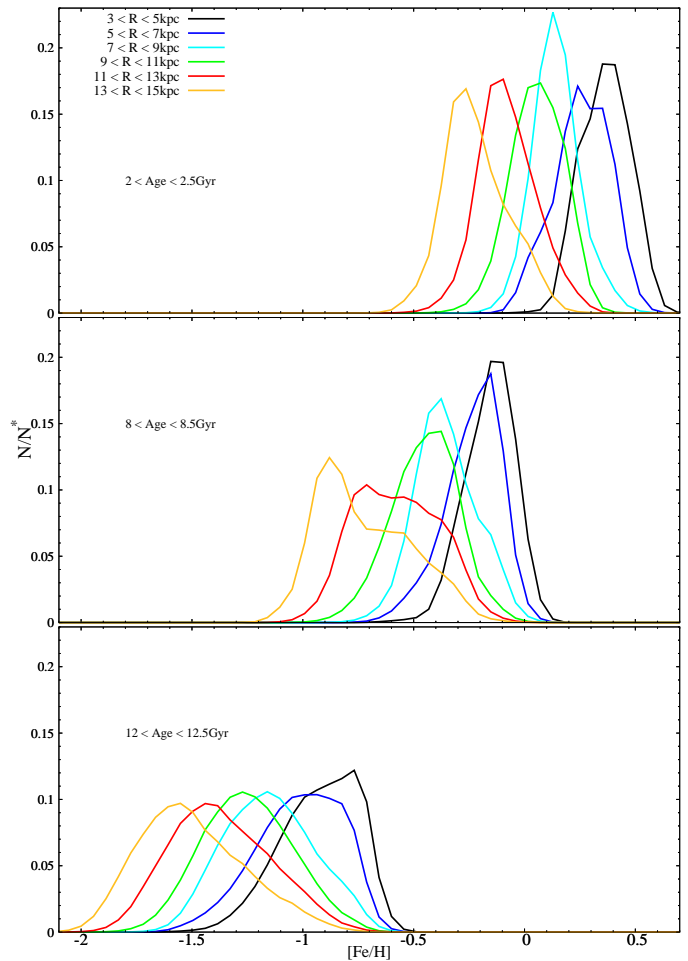


**Figure 16.** MDFs for three different age intervals. *Top*: for stars with  $2 < \text{Age} < 2.5$  Gyr. *Middle*: stars with  $8 < \text{Age} < 8.5$  Gyr. *Bottom*: stars with  $12 < \text{Age} < 12.5$  Gyr.

We have also compared our results with Casagrande et al. (2011) (cyan curves of our Figure 16 vs. the top panel of Casagrande’s Figure 16). While we also see the MDFs getting wider with time, the shift of our overall distribution is approximately  $-0.5$  dex in 5 Gyr, which is not compatible with their shift of approximately  $-0.1$  dex in 5 Gyr.

One thing in common for the sets of MDFs presented in Figure 16 is that, in spite of a clear mixing, there is a negative metallicity gradient for the three of them. This point is important because it tells us the stellar disc can experience significant radial migration while preserving a clear metallicity gradient. This means that one should not expect that radial migration is for sure able to erase a strong metallicity gradient.

This last point is also clear by plotting the same populations in the  $[\text{Fe}/\text{H}]$  vs.  $R$  plane, as shown in Figure 17. The stellar density at every radius shows a global metallicity gradient across the disc. Also, the width of the orange bands in the metallicity distribution is directly correlated with age. It is narrow for the youngest population, while it is wider for the sample of older stars, indicating a system

more dynamically evolved, and hence, a more mixed population.

## 10 DISCUSSION

Throughout this work, we have developed some ideas we consider relevant that we would like to highlight next.

Radial migration can produce an important effect in a galaxy and yet not be noticed with simple diagnostics such as a single abundance curve. Indeed, in spite of the fact that radial mixing is a global and general effect in disc galaxies, erasing the global metallicity gradient of a given galaxy requires powerful non-axisymmetric features in the disc; this does not seem to be the case for the MW, as deduced from a more suitable diagnostic to measure the impact of radial migration in the MW, like the MDFs. The MDFs seem to be a key observable to understand the radial migration effect in the MW, which in turn allows us to understand better the morphology of our galaxy. With an extensive set of detailed orbital simulations specifically adjusted to the MW, we conclude that the existence of a metallicity gradient in a given galaxy, does not rule out the presence of important radial mixing. Also, radial mixing in the external part of the Galaxy, is mainly due to the spiral arms and not to the bar; this means that similar spiral arms in a galaxy, would produce similar abundance curves and MDFs specifically towards the outskirts of the galaxy, independently of the existence of a bar. We find that the corotation resonance is able to produce a local flattening (around it) in the metallicity global curve (see Figures 9 and 17).

In order to reproduce the Galactic MDFs observed by Hayden et al. (2015), our simulations need 22% flatter Fe/H gradients during the last 5 Gyr of the evolution than the gradients predicted by the chemical evolution model (between 8 and 13 Gyr) of Carigi & Peimbert (2011). The current Fe/H slope predicted by the chemical evolution model is  $-0.102 \text{ dex kpc}^{-1}$  and its 22%-reduced slope is  $-0.080$ , for the gaseous component; for the stellar component, this becomes  $-0.063$ , which perfectly agrees with the Fe/H gradient from Cepheids ( $-0.062 \pm 0.002 \text{ dex kpc}^{-1}$ , Luck & Lambert 2011) in the 4-16 kpc range (however this work studies younger stars than the ones observed in the MDF APOGEE sample). The value of the reduced slope remains constant during the last 4.5 Gyr of the evolution, particularly in the 6-20 kpc range (see Fig. 5 by Carigi 1996).

In a chemical evolution model, a flatter Fe/H gradient implies a flatter O/H gradient by a similar proportion (Carigi 1996). As mentioned in Section 4, the chemical evolution model was built to reproduce the O/H gradient in the Galactic disc. The predicted O/H slope is equal to  $-0.057 \text{ dex kpc}^{-1}$  and its 22%-reduced slope is  $-0.045 \text{ dex kpc}^{-1}$  which is consistent with the  $-0.052 \pm 0.010 \text{ dex kpc}^{-1}$  value of García-Rojas & Esteban (2007), as well as with the O/H slope ( $-0.040 \pm 0.010 \text{ dex kpc}^{-1}$ ) by Esteban et al. (2013), when NGC 2579, an HII region at  $\sim 12.4 \text{ kpc}$ , was added to the sample of García-Rojas & Esteban (2007). In the chemical evolution model by Carigi & Peimbert (2011), a flatter O/H gradient can be obtained modifying the accretion rate; mainly, assuming a less intense inside-out scenario, i.e., taking into account a  $\tau(R)$  less dependent on  $R$ , which does not

affect the agreement with all chemical properties mentioned in Section 4.

Finally, we would like to emphasize that, although in our first attempt to fit the MDFs (Martinez-Medina et al. 2016), we utilised plain stellar birth radius as a proxy for metallicity (i.e. without a recipe for the chemical abundance distribution), we were able to closely approximate the MDF shapes, qualitatively speaking. However, it was not possible to fit the absolute magnitudes nor the width of the MDF; this is only possible with a combination between both approaches, dynamics and chemistry. Nonetheless, comparing qualitatively the MDF shapes constructed by using only the birth radius of the stars, we can see that the main factors that sculpt the MDFs in the outskirts of the Galaxy are the specific spiral arms morphology and dynamics. On the other hand, the initial metallicity gradient plays a fundamental role in the resulting shape of the inner MDFs, and becomes the main factor, even more important than the dynamical effect of the bar.

## 11 CONCLUSIONS

With a suitable combination of a detailed observationally motivated model of the Milky Way galactic potential, that includes spiral arms and bar, and a careful recipe to approximate the chemical evolution, we have performed an extensive set of chemodynamical simulations to study the history of the metallicity distribution function in the Galaxy.

Even when, in dynamical terms, radial migration does not leave a kinematical imprint in the stellar disc, the impact of the mechanism can be discerned from other observables, such as the metallicity distribution of the stellar disc.

By comparing the MDFs obtained from a set of Galactic models, by swapping their morphological and dynamical parameters, we show the sensitivity of the MDF shapes. This means that the shape of the MDF contains information of the spiral pattern as well as of the stellar disc dynamical evolution. In this work we provide the characteristics of the spiral arms that better fit the MDF shapes (Table 1).

Also, by tuning our simulated MDFs as close as possible to the observed ones, we introduce a method to set further constraints to chemical evolution models. This is helpful along the whole disc, but specially in the central region, where currently models do not provide information about the chemical content and its evolution.

We have quantified the reach of radial migration in moving stars away from their birth radius. For example, a considerable number of stars currently located at the solar circle were born at much smaller galactocentric distances. By inducing such extended radial excursions, migration explains how some stars exhibit a chemical content that does not correspond with the current location of a such star. In this manner, migration, mainly due to the spiral pattern, models the metallicity distribution across the disc, imprinting its morphology and dynamics on the MDFs.

Hundreds of strongly migrating stars that mimic closely the current solar orbital parameters are found. This shows that the solely study of radial migration would not be able to accurately constraint the birth place of the Sun. On the other hand, considering the low probability that the Sun was formed near its current galactocentric position, it may be, at

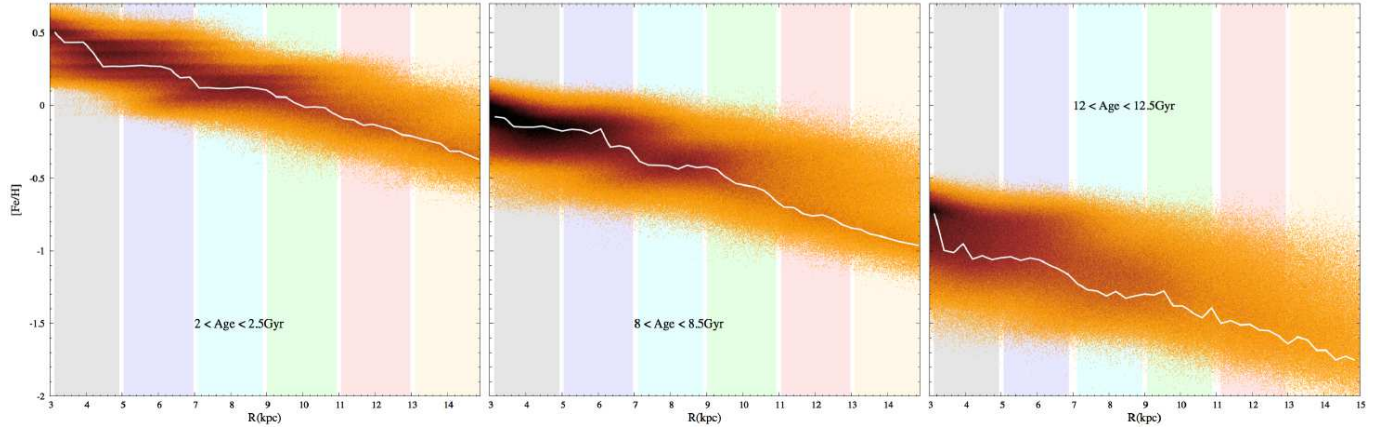


**Figure 17.** Distribution of stars in the plane  $[\text{Fe}/\text{H}]$  vs. Radius for populations of three different ages. The color code indicates density of stars, while the solid white lines are the mode of the  $[\text{Fe}/\text{H}]$  values at every radius.

least, inaccurate to employ the Sun as representative of the chemical abundances in the solar neighborhood; a better way to estimate the birth radius of the Sun, is to combine chemical and dynamical information. From our chemical model, we obtain a value of  $7.7 \pm 1$  kpc; from our dynamical simulations we obtain  $8.18 \pm 1.38$  kpc. When combining these two determinations, we obtain that the Sun was born at a galactocentric distance of  $7.9 \pm 0.8$  kpc.

We found that a dynamically evolved stellar population can exhibit a clear metallicity gradient regardless of the presence of important radial migration and heating in the disc. This means that the presence of important radial migration does not imply necessarily a substantial flattening of the metallicity gradient. Therefore, looking for flattened metallicity gradients is not a trustworthy method to establish the presence and importance of radial migration in galaxies.

By fitting the separation of the MDFs of the five radial bins presented by APOGEE, we find a galactic  $[\text{Fe}/\text{H}]$  abundance gradient of  $-0.080$  dex  $\text{kpc}^{-1}$ .

## ACKNOWLEDGEMENTS

We would like to acknowledge the anonymous referee for a careful review and several insightful suggestions. We acknowledge DGTIC-UNAM for providing HPC resources on the Cluster Supercomputer Miztli. L.A.M.M and B.P. acknowledge CONACYT Ciencia Básica grant 255167. DGAPA-PAPIIT through grants IN-114114 and IG-100115, L.A.M.M acknowledges DGAPA-PAPIIT through grant IN105916. A.P. acknowledges DGAPA-PAPIIT through grant IN-109716. L.A.M.M. acknowledges support from DGAPA-UNAM postdoctoral fellowship.

## REFERENCES

- Allen C., Santillán A., 1991, *Rev. Mex. Astron. Astrofis.*, 22, 255  
 Athanassoula, E. 2012, *MNRAS*, 426, L46  
 Berg, D. A., Skillman, E. D., Henry, R. B. C., Erb, D. K., & Carigi, L. 2016, *ApJ*, 827, 126  
 Boeche, C., Siebert, A., Piffl, T., et al. 2013, *A&A*, 559, A59  
 Boeche, C., Siebert, A., Piffl, T., et al. 2014, *A&A*, 568, A71  
 Brunetti, M., Chiappini, C., & Pfenniger, D. 2011, *A&A*, 534, A75  
 Carigi, L. 1996, *Rev. Mex. Astron. Astrofis.*, 32,  
 Carigi, L., & Peimbert, M. 2011, *Rev. Mex. Astron. Astrofis.*, 47, 139  
 Carlberg, R. G., Dawson, P. C., Hsu, T., & Vandenberg, D. A. 1985, *ApJ*, 294, 674  
 Casagrande, L., Schönrich, R., Asplund, M., et al. 2011, *A&A*, 530, A138  
 Comparetta, J., & Quillen, A. C. 2012, arXiv:1207.5753  
 Francois, P., & Matteucci, F. 1993, *A&A*, 280, 136  
 Edvardsson, B., Andersen, J., Gustafsson, B., et al. 1993, *A&A*, 275, 101  
 Esteban, C., Carigi, L., Copetti, M. V. F., et al. 2013, *MNRAS*, 433, 382  
 Freudenreich, H. T. 1998, *ApJ*, 492, 495  
 García-Rojas, J., & Esteban, C. 2007, *ApJ*, 670, 457  
 Gerssen, J., & Shapiro Griffin, K. 2012, *MNRAS*, 423, 2726  
 Grand, R. J. J., Kawata, D., & Cropper, M. 2012a, *MNRAS*, 421, 1529  
 Grand, R. J. J., Kawata, D., & Cropper, M. 2012b, *MNRAS*, 426, 167  
 Grenon, M. 1972, *IAU Colloq. 17: Age des Etoiles*, 55  
 Grenon, M. 1989, *Ap&SS*, 156, 29  
 Hayden, M. R., Bovy, J., Holtzman, J. A., et al. 2015, *ApJ*, 808, 132  
 Holmberg J., Nordstrom B., & Andersen J., 2009, *A&A*, 501, 941  
 Kawata, D., Grand, R. J. J., Gibson, B. K., et al. 2017, *MNRAS*, 464, 702  
 Kennicutt, R. C., Jr. 1998, *ApJ*, 498, 541  
 Kroupa, P., Tout, C. A., & Gilmore, G. 1993, *MNRAS*, 262, 545  
 Kubryk, M., Prantzos, N., & Athanassoula, E. 2013, *MNRAS*, 436, 1479  
 Lépine, J. R. D., Acharova, I. A., & Mishurov, Y. N. 2003, *ApJ*, 589, 210  
 Loebman, S. R., Roškar, R., Debattista, V. P., et al. 2011, *ApJ*, 737, 8  
 Loebman, S. R., Debattista, V. P., Nidever, D. L., et al. 2016, *ApJL*, 818, L6  
 Luck, R. E., & Lambert, D. L. 2011, *AJ*, 142, 136  
 Martínez-Barbosa, C. A., Brown, A. G. A., & Portegies Zwart, S. 2015, *MNRAS*, 446, 823  
 Martinez-Medina, L. A., Pichardo, B., Pérez-Villegas, A., & Moreno, E. 2015, *ApJ*, 802, 109  
 Martínez-Medina, L. A., Pichardo, B., Moreno, E., & Peimbert, A. 2016, *MNRAS*, 463, 459

- Mayor, M. 1974, *A&A*, 32, 321  
Minchev, I., & Famaey, B. 2010, *ApJ*, 722, 112  
Moreno, E., Pichardo, B., & Schuster, W. J. 2015, *MNRAS*, 451, 705  
Nieva, M.-F., & Przybilla, N. 2012, *A&A*, 539, A143  
Nordström, B., Mayor, M., Andersen, J., et al. 2004, *A&A*, 418, 989  
Peimbert, A., & Peimbert, M. 2010, *ApJ*, 724, 791  
Pichardo, B., Martos, M., Moreno, E. & Espresate, J., 2003, *ApJ*, 582, 230  
Pichardo, B., Martos, M., & Moreno, E. 2004, *ApJ*, 609, 144  
Pichardo, B., Moreno, E., Allen, C., et al. 2012, *AJ*, 143, 73  
Prantzos, N. 2009, *The Galaxy Disk in Cosmological Context*, 254, 381  
Roškar, R., Debattista, V. P., Quinn, T. R., Stinson, G. S., & Wadsley, J. 2008, *ApJL*, 684, L79  
Roškar, R., Debattista, V. P., Quinn, T. R., & Wadsley, J. 2012, *MNRAS*, 426, 2089  
Roškar R., Debattista V. P., & Loebman S. R., 2013, *MNRAS*, 433, 976  
Schönrich, R., & Binney, J. 2009a, *MNRAS*, 396, 203  
Schönrich, R., & Binney, J. 2009b, *MNRAS*, 399, 1145  
Schönrich, R., Binney, J., & Dehnen, W. 2010, *MNRAS*, 403, 1829  
Schönrich, R., & McMillan, P. J. 2017, *MNRAS*,  
Seabroke, G. M., & Gilmore, G. 2007, *MNRAS*, 380, 1348  
Sellwood J. A., Binney J. J., 2002, *MNRAS*, 336, 785  
Shevchenko, I. I. 2011, *ApJ*, 733, 39  
Spitoni, E., Romano, D., Matteucci, F., & Ciotti, L. 2015, *ApJ*, 802, 129  
Vera-Ciro, C., D’Onghia, E., Navarro, J., & Abadi, M. 2014, *ApJ*, 794, 173  
Wielen, R. 1977, *A&A*, 60, 263  
Wielen, R., Fuchs, B., & Dettbarn, C. 1996, *A&A*, 314, 438